Ni–Co–S–Se Alloy Nanocrystals: Influence of the Composition on Their in Situ Transformation and Electrocatalytic Activity for the Oxygen Evolution Reaction

Ni-Co-S-Se Alloy Nanocrystals: Influence of their Composition on their in-situ Transformation and Electrocatalytic Activity for the Oxygen Evolution Reaction

Mengjiao Wang[a,b] , Zhiya Dang[a], Mirko Prato[c], Dipak V. Shinde[a] Luca De Trizio,*[a] and Liberato Manna[a]*

[a]Nanochemistry Department and [c]Materials Characterization Facility, Istituto Italiano di Tecnologia (IIT), via Morego 30, 16163 Genova, Italy.

[b]Dipartimento di Chimica e Chimica Industriale, Università degli Studi di Genova, Via Dodecaneso 31, 16146 Genova, Italy.

KEYWORDS. Oxygen evolution reaction, turnover frequency, electrocatalysis, colloidal synthesis, quaternary alloy, tunable composition.

ABSTRACT

The electrocatalytic oxygen evolution reaction (OER) is an important half reaction in various technologies such as metal air batteries and electrochemical water splitting. Transition metal chalcogenides, especially those based on Co and Ni, are emerging as promising OER catalysts, thanks to their high activity and low cost. However, it is still being debated whether they act as actual catalysts or as catalyst precursors, undergoing structural and morphological changes under OER conditions. To gain a better comprehension of this topic, we have developed a simple colloidal synthesis method for alloy nanocrystals (NCs) based on Ni, Co, S and Se with a tunable composition, and we studied their structural and morphological evolution during OER. We found that binary CoSe, ternary Ni-Co-Se and quaternary Ni-Co-S-Se NCs, with the exception of NiSe, each undergo structural and morphological changes under OER conditions, forming the corresponding oxides/hydroxides which act as the actual active catalysts. Interestingly, we discovered that the composition of the starting metal chalcogenide NCs plays a major role in dictating the crystallinity, conductivity and activity of such oxide/hydroxide materials. This compositional tuning resulted in a ~ 7 fold improvement in the OER activity in terms of turnover frequency, from CoSe to $Ni_{0.25}Co_{0.65}S_{0.4}Se_{0.6}$ NCs. Our results suggest that the compositional engineering of metal chalcogenide materials could potentially be used to control their inevitable transformation into the corresponding oxide/hydroxide counterparts, eventually improving their OER activity.

Introduction

Electrochemical water splitting is becoming increasingly popular due to the global shift in energy production from non-renewable to renewable sources.[1-5] The electrocatalytic oxygen evolution reaction (OER) is an important half-reaction and an indispensable part of this process.[6-9] The development of efficient, stable, cost-effective OER catalysts is therefore extremely important. Although precious metal oxides such as IrO_2 and RuO_2 are highly active and stable for OER, their scarcity and high costs are driving scientific research toward more abundant and economic materials.[10-14] Over the last few decades, indeed, extensive efforts have been devoted to designing and synthesizing a great variety of electrocatalytic systems based on earth-abundant 3d transition metal compounds.[15-22] Among them, nickel- and cobalt-based chalcogenides have sparked great interest owing to their promising OER properties.[15, 23-27] Some examples are Ni-doped CoS_2 nanowires,[28] Co-doped NiSe nanowires,[29] $NiCo_2S_4$@graphene core@shell nanosheets,[30] Ni,Co-sulfide and Ni,Co-selenide microshperes,[31] Ni-Co-S nanosheets films,[32] Co-doped $NiSe_2$ nanoparticles films,[33] and $Co(S_xSe_{1-x})_2$ composites.[34]

Interestingly, it has been shown that the OER performances of such materials can be tuned via composition control, namely by modulating the Co/Ni elemental ratio in the catalyst. Liu et al. reported that the OER catalytic activity of $NiCo_2S_4$@graphene core@shell nanosheets was considerably higher than that of Ni_3S_4@graphene and Co_3S_4@graphene counterparts.[30] Xia et al. showed that Ni-doped $Co_{0.85}Se$ nanotube arrays were much more efficient and durable electrocatalysts in alkaline media than undoped $Co_{0.85}Se$.[35] In a recent study by our group, we also found that ternary $NiCoSe_4$ hollow microparticles exhibited an improved OER activity with respect to the binary $CoSe_2$ ones.[36] The improved performances observed in these cases have been tentatively explained by considering that the presence of both Ni and Co causes a

synergistic effect that can lead to the formation of more active sites with a lower activation energy.[37-39] Unfortunately, it is still unclear what the specific role of Ni and Co is in the OER, and what the optimal Ni/Co ratio is in each system. For example, in some recent works on Ni-Co chalcogenide materials, improved OER performances have been reported both in Co-rich[28, 36, 40] and in Ni-rich compounds.[29, 33] Also, as it has been documented in two recent studies, another interesting feature that characterizes Ni and Co chalcogenide based materials is that a synergistic effect may arise from the presence of both S and Se anions.[34, 41] Fang et al., for example, showed that peapod-like $Co(S_xSe_{1-x})_2$ nanoparticles have higher OER and HER performances than pure CoS_2 and $CoSe_2$ ones.[34] Moreover, Hu and co-workers recently demonstrated that the decoration of (NiCo)S/OH nanosheets with elemental Se can improve their OER activity.[41] However, a complete understanding of the roles of S and Se with regard to the catalytic properties of the final materials is still lacking.

Furthermore, it is still being debated whether these materials act as the actual catalysts or as pre-catalysts, which undergo a chemical transformation under OER conditions, thus forming metal oxides/hydroxides.[42] For example, Nath and co-workers reported that Ni_3Te_2, $FeNi_2Se_4$ and $NiSe_2$ do not undergo any degradation, oxidation or compositional change upon OER.[43-45] Conversely, Chen *et al.* systematically investigated the structural evolution of different transition metal dichalcogenides (MX, M = Co, Ni, Fe; X = S, Se, Te) under OER, and found that they all underwent oxidation under operational conditions, forming the corresponding metal oxides.[26] Similarly, Zhou *et al.* observed that Ni_3S_2 nanorods gradually transformed into hydrated nickel oxide when employed as OER catalysts.[46] Also, different authors reported that Ni-Co-S rods, NiSe nanowires and $NiCoSe_4$ hollow microcrystals were characterized by accumulated hydroxides or oxides species on their surface upon OER.[36, 42, 47-48] However, it is

still unclear which factors control the transformation of metal chalcogenide catalysts into their corresponding oxide/hydroxides.

All these recent findings have motivated us to investigate not only if optimized OER performances could be achieved via both a cation and anion composition tuning of Ni-Co-S-Se catalysts, but also what the specific roles of the Ni, Co, S and Se elements are. As no quaternary Ni-Co-S-Se NC systems have been reported to date, we first developed a new colloidal synthesis, which allowed us to produce binary NiSe and CoSe, ternary Ni-Co-Se and even quaternary Ni-Co-S-Se NCs which had the same crystal structure and comparable particle sizes (see Scheme 1).

Scheme 1. Sketch of the colloidal synthesis of ternary Ni-Co-Se and quaternary Ni-Co-S-Se alloy NCs having the same hexagonal crystal structure.

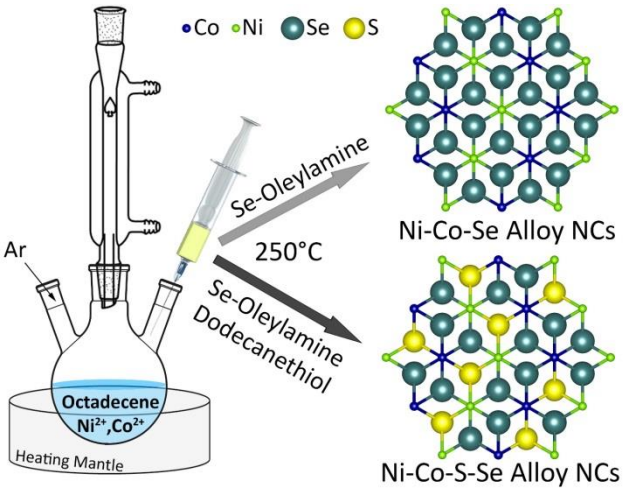

Then, we systematically studied the OER catalytic properties and transformations of such NCs during OER under alkaline conditions. Our findings revealed that Ni and Co based chalcogenide NCs, under OER conditions, completely transform into Co and/or Ni oxide/hydroxide materials, which are the actual active catalysts. It is of particular importance that the activity of such materials strongly depends on the composition of the starting chalcogenide NCs. According to

our findings, NiSe NCs had a poor activity since they did not form any Ni oxide or hydroxide species during the OER. CoSe NCs, on the other hand, completely transformed into active amorphous CoO_x and $Co(OH)_x$ materials. Ternary Ni-Co-Se NCs, upon OER, turned into amorphous Ni-Co oxides/hydroxides, which exhibited a higher catalytic activity than that of the Co oxides/hydroxides. Eventually, the insertion of S into Ni-Co-Se NCs, leading to Ni-Co-S-Se NCs, resulted in the formation of small Ni-Co oxide NCs (~1-2 nm in diameter) and $Co(OH)_2$ nanosheets (NSs) under OER conditions, and these had a higher activity than the ternary Ni-Co-Se NCs. We found that $Ni_{0.25}Co_{0.65}S_{0.4}Se_{0.6}$ was the optimal stoichiometry with regards to maximizing the final OER activity, with an onset potential of 262 mV and a OER current density of 10 mA/cm^2 at an overpotential of 358 mV. The TOF of that sample was measured to be 24.84 $\times 10^{-3}$ s^{-1} at an overpotential of 350 mV, which was ~7 times higher than that of the binary CoSe NCs.

Experimental section

Chemicals. Nickel(II) acetylacetonate [$Ni(acac)_2$, 95%], colbalt(II) acetylacetonate [$Co(acac)_2$, 99.99%], 1-Dodecanethiol (DDT, 98%), 1-Octadecene (ODE, 90%), oleylamine (OAm, 70%), ethanol (99.9%), toluene (99.7%), potassium hydroxide (KOH, 86%) and fluorine doped tin oxide (FTO) coated glass slides were purchased from Sigma-Aldrich. Selenium powder (99.99%) was purchased from Strem Chemicals. All the chemicals were used without any further purification.

Preparation of the Se Precursor. 8 mmol of Se powder was mixed with 24 mL of OAm in a 3-neck flask, and the resulting mixture was degassed under vacuum at 120 °C for 1 h. The system was slowly heated up to 230 °C for 3 h in an argon atmosphere until the solution became

transparent with an orange color. Eventually, the OAm-Se precursor solution was transferred to a glass vial and stored in an N_2 filled glovebox for further use.

Synthesis of Ni-Co-S-Se NCs. In a typical synthesis of Ni-Co-Se NCs, a desired amount of $Ni(acac)_2$ and $Co(acac)_2$ precursors (see Table 1 for details) was mixed with 10 mL of ODE in a3-neck flask and dried under vacuum for 1 h at 120 °C. Subsequently, 3 mL of the as-prepared OAm-Se solution (1 mmol of Se) was injected in an Ar atmosphere and the temperature was increased to 250 °C. After 5 min, the reaction mixture was immediately cooled down and quenched with toluene. The resulting NCs were washed twice by precipitation upon addition of ethanol followed by re-dispersion in toluene. Finally, the resulting black dispersion was stored in an N_2 filled glovebox for further use. In order to prepare quaternary Ni-Co-S-Se NCs, a certain amount of an S precursor (DDT) was injected just before the OAm-Se solution (see Table 1 for details). In this case, longer reaction times were required (see Table1).

Table 1. Synthetic parameters used for the synthesis of binary NiSe and CoSe, ternary Ni-Co-Se and quaternary $Ni_{0.25}Co_{0.75}S_{1-x}Se_x$ NCs. The composition of the samples was measured by Inductively Coupled Plasma elemental analysis.

Sample	$Ni(acac)_2$ (mmol)	$Co(acac)_2$ (mmol)	DDT (mL)	Reaction time (min)
CoSe	0	1	0	5
$Ni_{0.3}Co_{0.74}Se$	0.25	0.75	0	5
$Ni_{0.52}Co_{0.56}Se$	0.4	0.6	0	5
$Ni_{0.78}Co_{0.28}Se$	0.7	0.3	0	5
NiSe	1	0	0	5
$Ni_{0.3}Co_{0.73}S_{0.2}Se_{0.8}$	0.25	0.75	0.05	15
$Ni_{0.25}Co_{0.65}S_{0.4}Se_{0.6}$	0.25	0.75	0.1	60

Transmission Electron Microscopy (TEM) measurements. The samples were prepared by dropping dilute solutions of NCs onto carbon film-coated 200 mesh copper grids for low-resolution TEM and ultrathin carbon/holey carbon coated 400 mesh copper grids for high resolution TEM (HRTEM). Low-resolution TEM measurements were carried out on a JEOL-1100 transmission electron microscope operating at an acceleration voltage of 100 kV. For HRTEM, selected area electron diffraction (SAED) analyses and energy dispersive spectroscopy (EDS) were performed on a JEOL JEM-2200FS microscope equipped with a Schottky emitter operating at 200 kV, a CEOS spherical aberration corrector for the objective lens, an in-column energy filter (Omega-type), and a Bruker Quantax 400 EDS system with an XFlash 5060 detector.

X-ray diffraction (XRD). XRD patterns were obtained using a PANalytical Empyrean X-ray diffractometer equipped with a 1.8 kW Cu Kα ceramic X-ray tube and a PIXcel3D 2×2 area detector operating at 45 kV and 40 mA. The diffraction patterns were collected in air at room temperature using Parallel-Beam (PB) geometry and symmetric reflection mode. All XRD samples were prepared by drop casting a concentrated solution on a zero-background quartz substrate. XRD patterns were processed by HighScore 4.1 software from PANalytical and they were compared to the powder diffraction database from the inorganic crystal structure database (ICSD).

X-ray Photoelectron Spectroscopy (XPS). XPS analyses were obtained on samples before and after OER, using a Kratos Axis Ultra^{DLD} spectrometer equipped with monochromatic Al Kα source operated at 15 kV and 20 mA. Survey scan analyses were carried out with an analysis area of 300 x 700 microns and a pass energy of 160 eV. High resolution analyses were carried out with and the same analysis area and a pass energy of 20 eV. The Kratos charge neutralizer

system was used on all specimens. Spectra have been charge corrected to the main line of the carbon 1s spectrum (adventitious carbon) set to 284.8 eV. Spectra were analysed using CasaXPS software (version 2.3.17).

Elemental Analysis. This was carried out via Inductively Coupled Plasma Optical Emission Spectroscopy (ICP-OES) using an iCAP 6500 Thermo spectrometer. All chemical analyses performed by ICP-OES were affected by a systematic error of about 5%. Samples were dissolved in HCl/HNO_3 3:1 (v/v) for the analysis.

Electrochemical Measurements. The NCs that had been dispersed in toluene could be directly used as an ink to coat FTO substrates, without using any additives or binders. The electrodes were prepared by drop casting a solution containing 0.1 mg of NCs on 1 cm^2 FTO substrates and drying them in air. An IVIUM Compactstat was used for all the measurements. The electrochemical analysis was performed in a three-electrode system with an Ag/AgCl (3M NaCl) reference electrode, a Pt wire counter electrode and the NC coated FTO glasses as working electrodes. OER polarization curves were obtained in 1 M of KOH solution at a scan rate of 1 mV/s by linear sweep voltammetry (LSV). Scans were repeated until reproducible curves were observed. All the potentials were measured versus Ag/AgCl (3M NaCl) and converted to the reversible hydrogen electrode (RHE) potential scale using the following formula:

$E_{RHE} = E_{Ag/AgCl} + 0.197 + 0.059*pH.$

To compare the catalytic activity of the different catalysts as accurately as possible, the polarization curves were corrected for ohmic losses throughout the system by using Iviumsoft to get the final iR-corrected data. The impedance spectra of the electrodes were measured at open

circuit potentials in a frequency range from 0.1 Hz to 10000 Hz at a sinusoidal amplitude of 5 mV.

TOF calculations: The TOF was calculated using following formula

$$\text{TOF} = \frac{jS}{4Fn}$$

in which, j is the measured current density (mA/cm^2), S is the geometric surface area of the FTO electrode, F is Faraday's constant (96485.3 C/mol), and n is the moles of the metal atom (Ni+Co) in the loaded catalysts. The number 4 in the TOF calculation means 4 electron transfers per O_2 molecule evolution

Results and discussion

We first synthesized binary and ternary Ni-Co-Se NCs with CoSe, $Ni_{0.3}Co_{0.74}Se$, $Ni_{0.52}Co_{0.56}Se$, $Ni_{0.78}Co_{0.28}Se$ and NiSe compositions, as was revealed by our ICP elemental analysis (see Table 1). The TEM images of the samples, which are reported in Figure 1, indicated that the size of the NCs was around 10 nm in all cases except for NiSe NCs, which exhibited a mean diameter of 25 nm. Our XRD analysis revealed that all the NC products had the same hexagonal crystal structure, with no presence of secondary phases (see Figure 1f). In more detail, the XRD patterns of both NiSe and CoSe NCs well matched those of bulk hexagonal NiSe (ICSD number 29310) and CoSe (ICSD number 53959), respectively, while the reflections that were observed for Ni-Co-Se NCs were systematically located between those of the CoSe and NiSe hexagonal structures, suggesting the formation of alloyed NCs (see Figure 1f): the increase in the Ni content in Ni-Co-Se NCs led to a shift of the XRD peaks toward lower 2-theta values, indicating an expansion of the lattice parameters. This is in agreement with the larger unit cell of hexagonal NiSe (a=3.66 Å, c=5.33 Å) compared to that of CoSe (a=3.594 Å, c=5.277 Å).

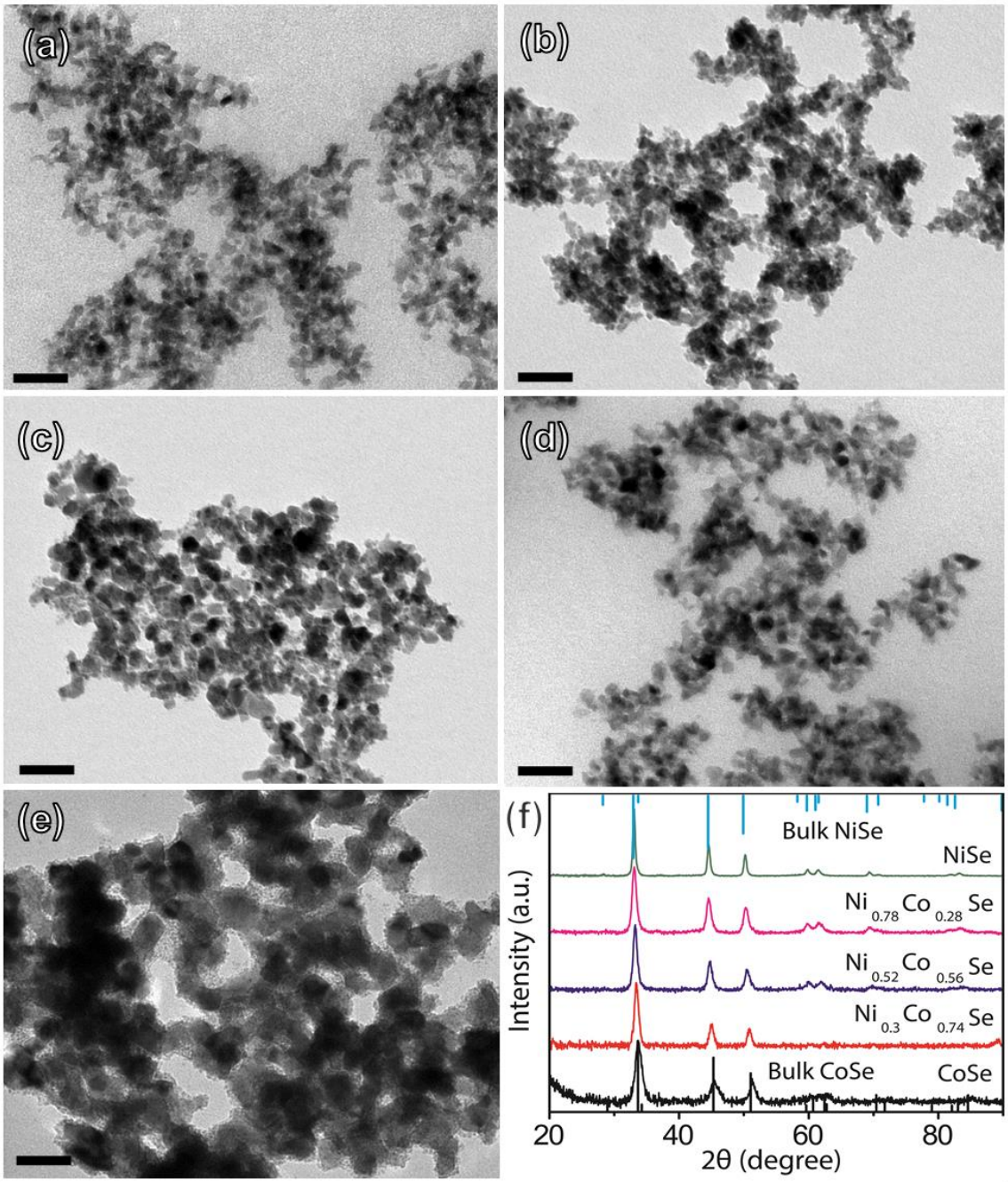

Figure 1. (a-e) TEM images and (f) XRD patterns of (a) CoSe, (b) $Ni_{0.3}Co_{0.74}Se$, (c) $Ni_{0.52}Co_{0.56}Se$, (d) $Ni_{0.78}Co_{0.28}Se$ and (e) NiSe NCs. The scale bar in each panel is 50 nm. (f) The bulk reflections of hexagonal NiSe (ICSD number 29310) and CoSe (ICSD number 53959) are also reported by means of light blue and black bars, respectively.

The synthesized NCs were deposited on FTO substrates and their electrocatalytic OER properties were evaluated (see the Experimental Section for details). The resulting polarization curves are reported in Figure 2a. It is evident that the onset potentials for the OER heavily depend on the composition of the NCs. In particular, NiSe NCs exhibited the highest onset potential, which systematically decreased when the amount of Co increased, reaching the lowest value of 272 mV in the $Ni_{0,3}Co_{0,74}Se$ composition (see Figure 2a, red curve). This value then raised to 317 mV in the samples with no Ni, i.e. in the CoSe NCs (see Figure 2a, black curve). In order to elucidate the underlying OER mechanism, the obtained LSV plots were fitted using the Tafel equation.[27, 49] From the Tafel plots, which are reported in Figure 2b, the Tafel slopes for CoSe and $Ni_{0.3}Co_{0.74}Se$ were calculated to be ~67 and ~76 mV/dec, respectively, indicating that $Ni_{0.3}Co_{0.74}Se$ NCs have slightly slower OER kinetics than CoSe NCs. The Tafel slopes of the $Ni_{0.52}Co_{0.56}Se$, $Ni_{0.78}Co_{0.28}Se$ and NiSe samples were ~83, ~184 and ~286 mV/dec, respectively, i.e. they had slower OER kinetics than the $Ni_{0.3}Co_{0.74}Se$ and CoSe samples (see Table2). It is worth to highlight here that since LSV measurements were conducted at a very low scan rate (1 mV/s), any capacitive contribution to the measured OER currents should be minimal. The specific activity of the catalysts was evaluated by TOF calculation, which refers to the rate of O_2 molecules that evolved per metal atom per second. Figure 2c and Table 2 demonstrate that the TOF improved up to three times upon the optimization of the ternary Ni-Co-Se NCs' composition. The CVs of samples measured at a sweep rate of 10 mV/s are provided in Figure S4a of the SI to better explain the observed improvements in the OER. It can be seen that the best performing sample shows the largest pseudocapacitive peaks, indicating the increase of the electrochemically active surface area of the catalyst. On the other hand, the NiSe NCs did not

show any pseudocapacitive peak in the same range, indicating that no formation of Ni oxide species took place, thus explaining the observed poor performance of NiSe NCs in the OER.[21]

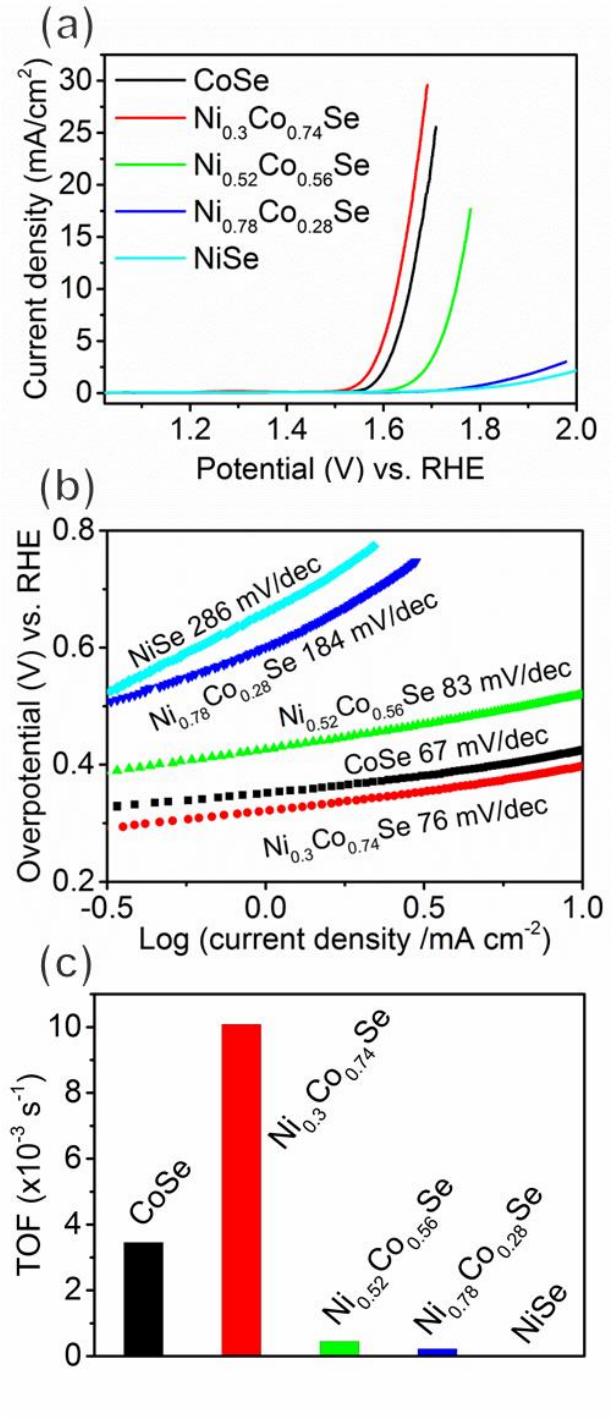

Figure 2. (a) LSVs measured at a sweep rate of 1 mV/s, (b) Tafel plots and (c) TOF values at η = 0.35 V of binary and ternary Ni-Co-Se NCs.

Table 2. Various electrochemical parameters of Ni-Co-Se-FTO electrodes.

Sample	Onset potential (mV)	η/mV at j = 10 mA/cm^2	Tafel slope (mV/dec)	Rs (Ω)/cm^2	TOF (× 10^{-3} s^{-1})
CoSe	317	425	67	12.9	3.46
$Ni_{0.3}Co_{0.74}Se$	277	397	76	11.2	10.09
$Ni_{0.52}Co_{0.56}Se$	383	520	83	14.2	0.45
$Ni_{0.78}Co_{0.28}Se$	504	-	184	14.8	0.23
NiSe	507	-	286	16.4	0.04

Furthermore, our impedance spectroscopy analyses indicated that the series resistance (R_s) of the samples decreased from 12.9 Ω for CoSe NCs to 11.2 Ω for $Ni_{0.3}Co_{0.74}Se$ NCs, before rising again at higher Ni contents (see Table 2). Since all other parameters were kept constant in all cases, the observed R_s of the systems could be considered to be directly related to the electrical conductivity of the NCs. Thus, we concluded that the incorporation of an optimal amount of Ni in CoSe NCs (reaching a Ni/Co ratio of 1/2.4) led not only to an increase in the overall electrical conductivity of the sample, but also to a decrease of the onset potential for the OER. These results are in line with the study of Bates *et al*., in which they observed improvements in the OER properties when going from Ni-oxide to Ni,Co-oxide catalysts, most likely as a consequence of the better electrical conductivity of the latter.[20, 50-51]

In order to better understand the composition and the structure of the actual active catalyst, we also carried out XRD and ICP elemental analyses of representative CoSe, $Ni_{0.3}Co_{0.74}Se$ and NiSe

NC samples after performing the OER. The XRD patterns of the cycled CoSe and $Ni_{0.3}Co_{0.74}Se$ NCs exhibited no diffraction peaks, apart from those which were related to the substrate, while the NiSe NCs retained their hexagonal structure (see Figure 3c). These results were consistent with what was observed during ICP elemental analysis: after the OER, NiSe NCs preserved their original stoichiometry, whereas no residual Se was found in the CoSe and $Ni_{0.3}Co_{0.74}Se$ samples, in which Co and/or Ni were the only elements detected. It should be noted that we measured the Ni/Co ratio of the $Ni_{0.3}Co_{0.74}Se$ NCs before and after the OER, and it was found to be constant. To have a better understanding of the chemical, structural and morphological evolution of the $Ni_{0.3}Co_{0.74}Se$ NC upon OER, we also performed XPS and HRTEM analyses. TEM micrographs of the starting $Ni_{0.3}Co_{0.74}Se$ sample indicated that the as synthesized NCs are monocrystalline and they exhibit the expected hexagonal crystal structure, as revealed by XRD (see Figure 3b,c and Figure S1 of the SI). Moreover, the STEM-EDS elemental mapping revealed a uniform distribution of Ni, Co and Se elements in the NCs (Figure 3c). However, a profound restructuring of the NCs was observed after the OER: the HRTEM analyses evidenced the presence of a major fraction of amorphous Ni, Co- based nanoparticles and a minor fraction of NCs whose crystal structure could be ascribed either to cubic CoO or NiO (ICSD numbers 9865 and 9866, respectively), as these two structures have similar lattice parameters (see Figure 3d,e and Figure S2 of the SI). Furthermore, STEM-EDS elemental mapping revealed that these particles only contained Ni, Co and O (with a Ni/Co ratio of 1/2.4), but no Se, confirming what had already been measured by ICP (see Figure 3fand Figure S9 of the SI). XPS analyses of ternary NCs before and after OER further confirmed our findings: while the Se signal disappeared upon OER, the position of the Ni and Co peaks shifted to higher binding energies, suggesting the evolution of the catalyst from Ni-Co-Se to Ni-Co oxide/hydroxide materials (see Figure S10 of the SI).

These results are in agreement with those reported by different groups, who observed the transformation of MX nanostructures (MX, M = Co, Ni, Fe; X = S, Se, Te) into the corresponding metal oxides/hydroxides upon OER in alkaline conditions.[42, 46-48] The oxidation process, at the same time, was shown to affect the chalcogen anions, which are released from the starting nanostructures in the form of SeO_x or SO_x species.[26, 42, 48, 52-53] In order to study the fate of organic ligands we performed a Fourier transform infrared spectroscopy study on a Ni-Co-Se NC film before and after five CVs of OER (see Figure S11 of the SI for details). What we observed is that the native ligands (*i.e.* oleylamine) were present on our catalyst even after OER. This finding suggests that oleylamine molecules, which are not soluble in the electrolyte, most likely bind to Ni and Co oxide/hydroxide species that form upon the transformation of native Ni-Co-Se NCs.

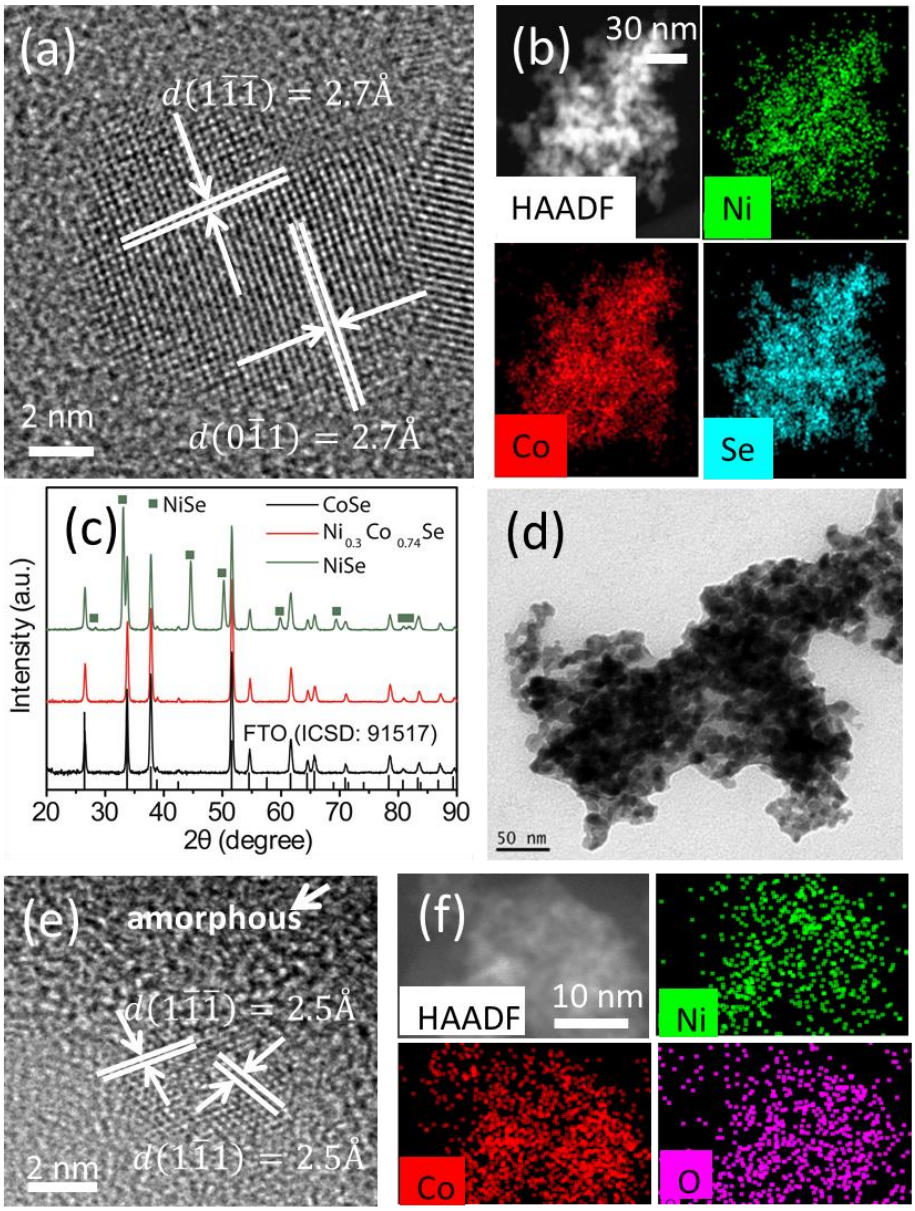

Figure 3. (a) HRTEM image of $Ni_{0.3}Co_{0.74}Se$NCs before OER, exhibiting the expected hexagonal CoSe crystal structure and characterized by the absence of crystal defects. (b) EDS elemental mapping of a group of $Ni_{0.3}Co_{0.74}Se$NCs. (c) XRD patterns of CoSe, $Ni_{0.3}Co_{0.74}Se$ and NiSe NCs on FTO substrates after OER. (d) TEM image and (e) HRTEM image of $Ni_{0.3}Co_{0.74}Se$NCs after OER, showing the presence of both amorphous particles and a small fraction of tiny CoO or NiO NCs. (f) EDS elemental mapping of $Ni_{0.3}Co_{0.74}Se$ NCs after OER.

Overall, our findings indicate that Ni-Co-Se NCs underwent a phase transformation under OER conditions, releasing Se anions and forming mainly amorphous Ni-Co oxide/hydroxide species, which were the actual catalytic materials.[22, 31, 42, 46-48, 54-58] The OER performance of such species depended on their relative composition: an optimal Ni/Co ratio was the key parameter not only to increasing the conductivity and the number of active sites of the final material, but also to lowering its onset potential. However, the NiSe NCs did not undergo any phase changes and they retained their crystal structure under OER conditions. In this case, differently from what observed by other groups, no active Ni oxide/hydroxide species were found, explaining the poor performance of our NiSe NCs in the OER.[42, 48, 55, 59]

Quaternary Alloy NC Systems

We further synthesized quaternary Ni-Co-S-Se NCs in order to investigate the effects of the presence of sulfur on the final OER performance of such compounds. While keeping the Ni/Co ratio fixed to 1/2.4, which was found to optimize the catalytic activity of Ni-Co-Se NCs, we synthesized quaternary $Ni_{0.3}Co_{0.73}S_{0.2}Se_{0.8}$ and $Ni_{0.25}Co_{0.65}S_{0.4}Se_{0.6}$ NCs by using the same colloidal procedure but varying the relative amount of S and Se precursors (see the Experimental Section and Table 1). The produced NCs had a mean size of 10 nm, as was determined by TEM analysis (see Figure 1b), and the same hexagonal crystal structure as the binary and ternary Ni-Co-Se NCs (see Figure 4c). A systematic shift of the XRD peaks toward larger 2-theta values was observed when the relative amount of S inside the NCs was increased. This is consistent with the ionic radius of S, which is smaller than that of Se, suggesting the formation of alloyed structures. It is important to underline here that a further inclusion of S inside the alloy NCs, above the $Ni_{0.25}Co_{0.65}S_{0.4}Se_{0.6}$ composition, led to quaternary NCs having a cubic structure (see Figure S2 of the SI). However, these samples were excluded from our study since our final goal

was to compare the catalytic properties of NC systems with different compositions but having the same crystal structure.

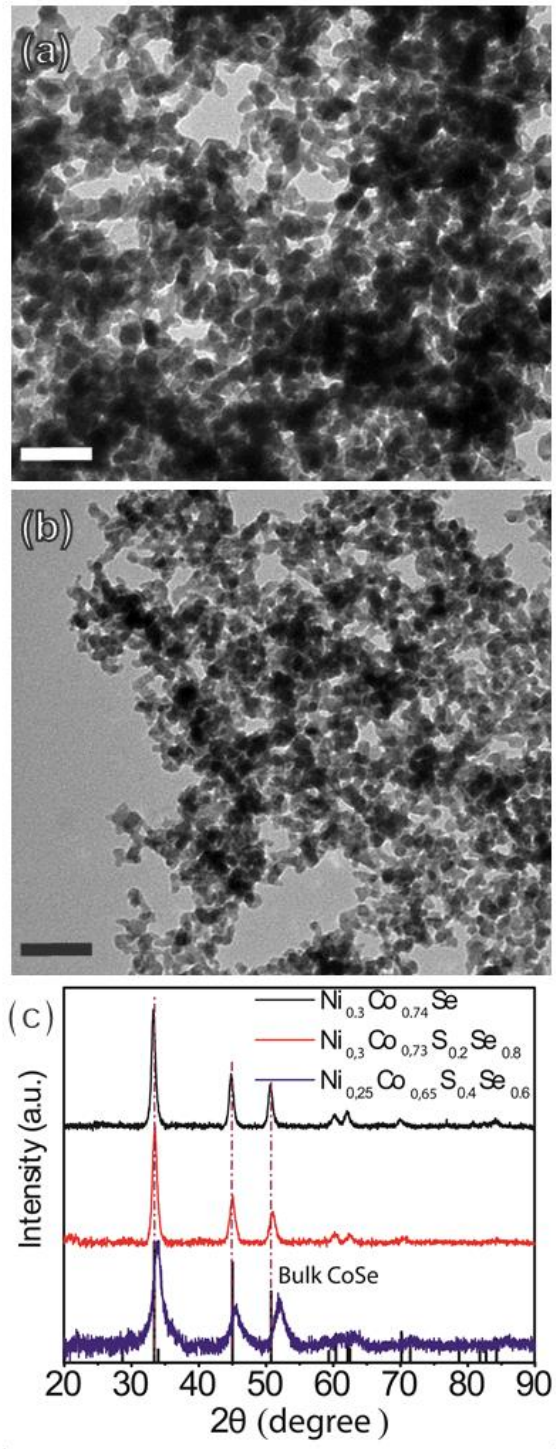

Figure 4. Low resolution TEM images of (a) $Ni_{0.3}Co_{0.73}S_{0.2}Se_{0.8}$ and (b) $Ni_{0.25}Co_{0.65}S_{0.4}Se_{0.6}$NCs. The scale bar is 50 nm. (c) XRD patterns of $Ni_{0.3}Co_{0.74}Se$, $Ni_{0.3}Co_{0.73}S_{0.2}Se_{0.8}$ and $Ni_{0.25}Co_{0.65}S_{0.4}Se_{0.6}$ NCs. The pattern of $Ni_{0.3}Co_{0.74}Se$ NCs is also reported for a better comparison.

The electrocatalytic OER properties of quaternary alloy NCs were evaluated by LSV, and the corresponding polarization curves are shown in Figure 5a. It is evident that the introduction of S inside the ternary Ni-Co-Se NCs resulted in an improved OER activity. The electrodes that were composed of $Ni_{0.3}Co_{0.73}S_{0.2}Se_{0.8}$ and $Ni_{0.25}Co_{0.65}S_{0.4}Se_{0.6}$ NCs exhibited a high activity for OER, with an onset overpotential of about 272 mV and 262 mV, respectively (see Table 3). The Tafel slopes of the $Ni_{0.3}Co_{0.73}S_{0.2}Se_{0.8}$ (64 mV/dec) and $Ni_{0.25}Co_{0.65}S_{0.4}Se_{0.6}$ (64 mV/dec) NCs were lower than that of the $Ni_{0,3}Co_{0,74}Se$ (76 mV/dec) NCs, suggesting that the quaternary systems had faster OER kinetics (see Figure 5b). Furthermore, the calculated TOF (Figure 5c) of the $Ni_{0.25}Co_{0.65}S_{0.4}Se_{0.6}$ NCs at an overpotential of 0.35 V was more than twice that of the $Ni_{0,3}Co_{0,74}Se$ NCs. In addition, the impedance analysis showed that the R_s of the $Ni_{0.3}Co_{0.73}S_{0.2}Se_{0.8}$ (8.9 Ω) and $Ni_{0.25}Co_{0.65}S_{0.4}Se_{0.6}$ (7.4 Ω) NCs were much smaller than that of the $Ni_{0,3}Co_{0,74}Se$ NCs (11.2 Ω), further supporting that quaternary systems are characterized by a faster charge transfer (see Table 3). These results confirmed that$Ni_{0.25}Co_{0.65}S_{0.4}Se_{0.6}$ NCs had the highest intrinsic catalytic activity among all the reported samples, and further stability tests revealed that they also have a stable OER performance (see Figure S3 of the SI).

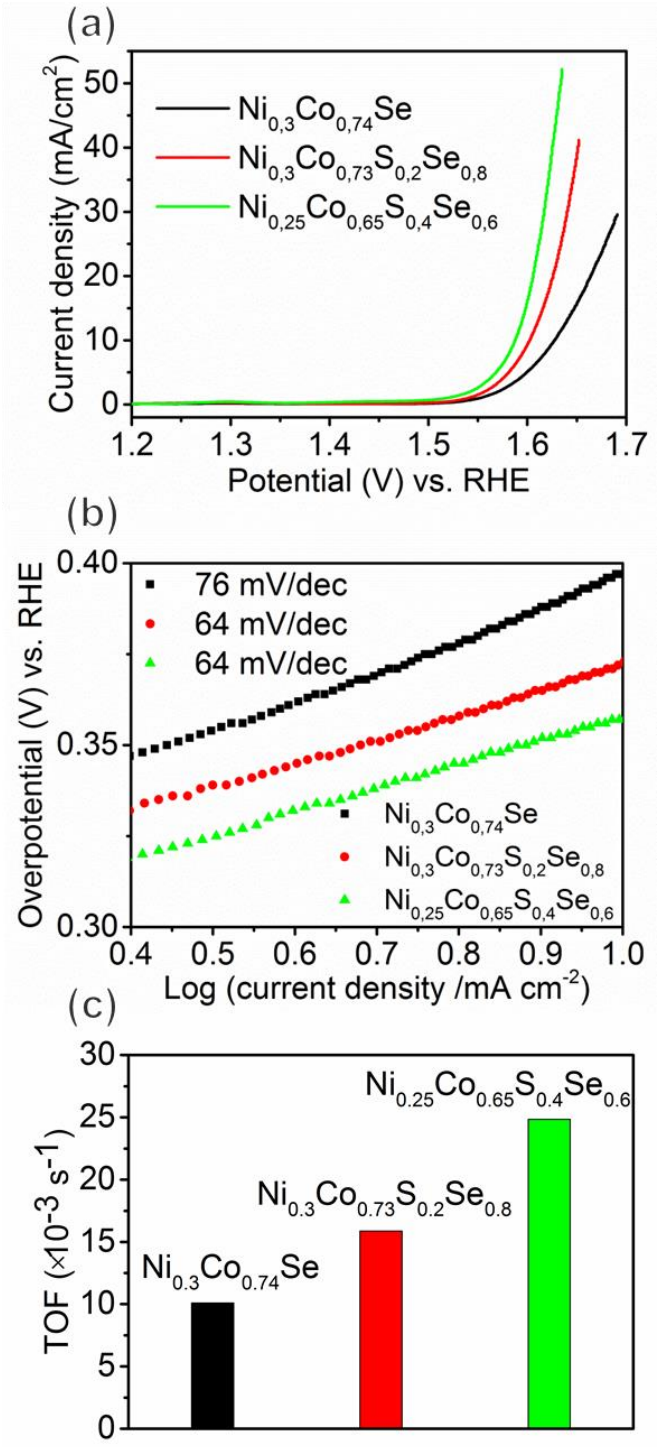

Figure 5. (a) LSVs measured at a sweep rate of 1 mV/s, (b) Tafel plots and (c) TOF values at η = 0.35 V of ternary and quaternary Ni-Co-S-Se NCs with various compositions.

Table 3. Summary of electrochemical OER parameters of quaternary Ni-Co-S-Se NC catalysts.

Sample	Onset potential (mV)	η/mV at j = 10 mA/cm^2	Tafel slope (mV/dec)	Rs (Ω)/cm^2	TOF ($\times 10^{-3}$ s^{-1})
$Ni_{0.3}Co_{0.74}Se$	277	397	76	11.2	10.05
$Ni_{0.3}Co_{0.73}S_{0.2}Se_{0.8}$	272	373	64	8.9	15.88
$Ni_{0.25}Co_{0.65}S_{0.4}Se_{0.6}$	262	358	64	7.4	24.84

To further elucidate the reasons underlying the better OER performance of $Ni_{0.25}Co_{0.65}S_{0.4}Se_{0.6}$ NCs, polarization curves of all the samples were also collected between 1.0 and 2.0 V versus RHE at a scan rate of 10 mVs^{-1}. As shown in Figure S4b, the CVs of all the samples were characterized by one broad anodic peak in the range of 1.2-1.4 V (versus RHE). As mentioned above in the discussion of the ternary Ni-Co-Se samples, the presence of this single peak stands for the oxidation of Ni^{II} to Ni^{III} or Ni^{IV}.The increase in the intensity of this redox peak when going from $Ni_{0,3}Co_{0,74}Se$ to $Ni_{0.25}Co_{0.65}S_{0.4}Se_{0.6}$ NCs suggested that quaternary NC samples are characterized by a higher amount of Ni^{II} sites which can undergo a reversible redox reaction to Ni^{III} or Ni^{IV}. These sites might act as catalytically active sites, which would explain the superior electrocatalytic performance of our quaternary samples.[60-61]

HRTEM studies were carried out on $Ni_{0.25}Co_{0.65}S_{0.4}Se_{0.6}$ NCs before and after OER so that the chemical and structural evolution of the NCs could be further studied. Before OER, the NCs were found to have the expected hexagonal crystal structure and a homogeneous distribution of the four elements, with a mean composition of $Ni_{0.3}Co_{0.63}S_{0.4}Se_{0.6}$, which is in agreement with ICP results (see Figure 6a, c and Figure S5 of the SI). Interestingly, our HRTEM analysis also revealed that quaternary NCs were characterized by a large amount of crystal defects including steps (see Figure 6c), twin boundaries (see Figure 6b, d, e) and stacking faults (see Figure 6e,

and see Figure S6 of the SI for more examples). The formation of these defects is tentatively explained by the presence of S anions on the Ni-Co-Se hexagonal lattice, which could induce a compressive strain, since the ionic radius of S is smaller than that of Se (184pm compared to 198pm). However, a large number of small NiO or CoO NCs, amorphous Ni, Co oxide/hydroxide nanoparticles and $Co(OH)_2$ ultrathin nanosheets were detected after the OER by HRTEM analysis (see Figure 6i, j, Figure S7 of the SI). Indeed, the STEM-EDS elemental mapping of the final sample confirmed the presence of Ni, Co and O elements, but there were almost no traces of S and Se (the ratio of (S+Se)/(Ni+Co) was 5.3%). Such findings were also supported by the XRD and XPS analyses of the $Ni_{0.25}Co_{0.65}S_{0.4}Se_{0.6}$NC sample after the OER, which revealed the presence of a fraction of crystalline $Co(OH)_2$ (ICSD number 53994) (see Figure S8 of the SI). XPS analyses of quaternary NCs before and after OER, also in this case corroborated our findings: while the S and Se signals disappeared upon OER, the position of Ni and Co peaks shifted to higher binding energies, suggesting the evolution of the catalyst from Ni-Co-Se-S to Ni-Co oxide/hydroxide species (see Figure S10 of the SI). We believe that the preferential formation of such crystalline oxide/hydroxide nanoparticles could be directly correlated to the presence of crystal defects in the parent $Ni_{0.25}Co_{0.65}S_{0.4}Se_{0.6}$ NCs, which might act as preferential nucleation sites.

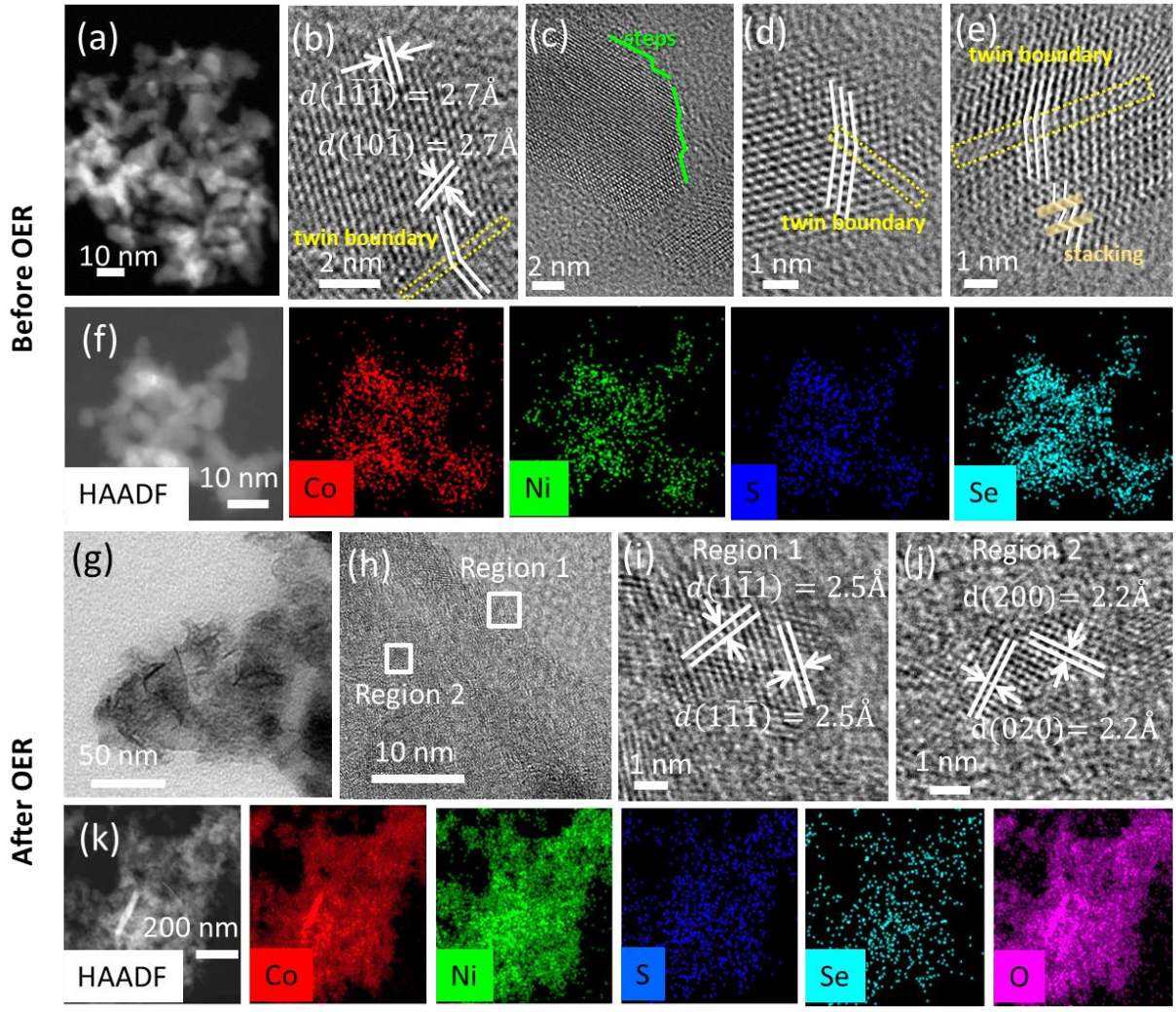

Figure 6. (a) HAADF-STEM image, (b-e) HRTEM images and (f) EDS elemental mapping of $Ni_{0.25}Co_{0.65}S_{0.4}Se_{0.6}$ NCs before OER. The NCs exhibit the expected hexagonal structure (ICSD number 53959) and they are characterized by a rich presence of defects. (g) TEM micrograph, (h) HRTEM image of $Ni_{0.25}Co_{0.65}S_{0.4}Se_{0.6}$NCs after OER. (i,j) Two regions of panel (h) are magnified to show the lattice fringes of the oxide NCs, which matching either NiO (ICSD number 9866) or CoO (ICSD number 9865). (k) EDS elemental mapping of $Ni_{0.25}Co_{0.65}S_{0.4}Se_{0.6}$ NCs after OER.

Overall, our findings indicated that both ternary and quaternary Ni-Co-S-Se NCs undergo oxidation upon OER and transform *in situ* into Ni, Co oxide/hydroxide materials. Ternary samples were found to form active amorphous compounds, while quaternary NCs transformed mostly into small NiO/CoO NCs and ultrathin $Co(OH)_2$ nanosheets. Thus, we ascribe the superior OER performance of Ni-Co-S-Se NCs to the crystalline species which were experimentally found to promote the catalytic activity of the final catalyst.[62] It is also important to highlight here that our electrochemical results have been obtained using Pt counter electrodes in the experimental setup. Our ICP, STEM-EDS and XPS elemental analyses performed on both ternary and quaternary compounds before and after OER indicated the absence of Pt in both the catalyst and the electrolyte, excluding any influence of Pt on the catalytic properties and on the transformations of the NCs (see Figure S9 and S10 of the SI).

Conclusions

In conclusion, we have developed a colloidal synthesis method to produce binary NiSe, CoSe, ternary Ni-Co-Se, and quaternary Ni-Co-S-Se NCs with controllable compositions and identical hexagonal crystal structures. We studied, in detail, variations in the OER catalytic activity of these NC systems as a function of their composition. We observed that, under OER conditions, both ternary Ni-Co-Se and quaternary Ni-Co-S-Se NCs NC samples underwent a complete chemical transformation, losing the chalcogen anions and forming Ni, Co oxides/hydroxide compounds, which are the actual catalytic species for OER. While the oxidation of metal chalcogenides upon OER has been reported by different authors, not much is known on how the composition and the structure of starting materials affect this process and the properties of the resulting active compounds. What we found is that the crystallinity and activity of the oxide/hydroxide products are strongly dependent on the composition of the starting NCs.

In more detail, when working with Ni-Co-Se NCs, amorphous Ni, Co oxides/hydroxide nanoparticles were mainly produced. Interestingly, the activity of such species was found to be optimal at a Ni/Co ratio of 1/2.4. The addition of S to the ternary compounds, thus forming quaternary alloy Ni-Co-S-Se NCs, led to a systematic improvement in the final OER activity. We found that the presence of S resulted in the formation of crystal defects inside the alloy NCs. Such defects, in turn, acted as preferential nucleation sites for the formation of small NiO-CoO NCs and ultrathin $Co(OH)_2$ nanosheets during the OER, and these species/compouds are believed to have promoted the final OER performance of the catalyst.

Our work highlights that a deep characterization of the catalytic materials upon OER is of fundamental importance in order to understand their evolution under operational conditions. Indeed, we have proved here that the chemical and structural properties of the active species which form in-situ strongly depend on the composition and the crystal phase of the starting catalytic material.

ASSOCIATED CONTENT

Supporting information

SAED patterns of $Ni_{0.3}Co_{0.74}Se$ NCs before and after OER, XRD patterns of $Ni_{0.42}Co_{0.38}S_{0.68}Se_{0.32}$ NCs, the stability test of $Ni_{0.25}Co_{0.65}S_{0.4}Se_{0.6}$ NCs, CVs of ternary and quaternary NCs with various compositions, SAED patterns of $Ni_{0.25}Co_{0.65}S_{0.4}Se_{0.6}$ NCs before and after OER, additional HRTEM images of $Ni_{0.25}Co_{0.65}S_{0.4}Se_{0.6}$ NCs before and after OER, XRD pattern of $Ni_{0.25}Co_{0.65}S_{0.4}Se_{0.6}$ NCs on an FTO substrate after OER, STEM-EDS spectra of $Ni_{0.3}Co_{0.74}Se$ and $Ni_{0.25}Co_{0.65}S_{0.4}Se_{0.6}$ NCs after OER, XPS spectra of $Ni_{0.3}Co_{0.74}Se$ and $Ni_{0.25}Co_{0.65}S_{0.4}Se_{0.6}$ NCs before and after OER.

AUTHOR INFORMATION

Corresponding Authors

*E-mail: luca.detrizio@iit.it

*E-mail: dipak.shinde@iit.it

Notes

The authors declare no competing financial interest.

ACKNOWLEDGMENT

We acknowledge funding from the European Union under grant agreements n. 614897 (ERC Grant TRANS-NANO). We thank Irene Rosina for her support in the Fourier transform infrared spectroscopy analysis.

REFERENCES

1. Suen, N. T.; Hung, S. F.; Quan, Q.; Zhang, N.; Xu, Y. J.; Chen, H. M., Electrocatalysis for the Oxygen Evolution Reaction: Recent Development and Future Perspectives. *Chem. Soc. Rev.* **2017,** *46* (2), 337-365.

2. Song, S.; Zhang, H.; Ma, X.; Shao, Z.; Baker, R. T.; Yi, B., Electrochemical Investigation of Electrocatalysts for the Oxygen Evolution Reaction in PEM Water Electrolyzers. *Int. J. Hydrogen Energy* **2008,** *33* (19), 4955-4961.

3. Deng, X.; Tüysüz, H., Cobalt-Oxide-Based Materials as Water Oxidation Catalyst: Recent Progress and Challenges. *ACS Catal.* **2014,** *4* (10), 3701-3714.

4. Xu, Q.; Jiang, H.; Zhang, H.; Jiang, H.; Li, C., Phosphorus-Driven Mesoporous Co_3O_4 Nanosheets with Tunable Oxygen Vacancies for the Enhanced Oxygen Evolution Reaction. *Electrochim. Acta* **2018,** *259*, 962-967.

5. Wu, J.; Subramaniam, J.; Liu, Y.; Geng, D.; Meng, X., Facile Assembly of $Ni(OH)_2$ Nanosheets on Nitrogen-Doped Carbon Nanotubes Network as High-Performance Electrocatalyst for Oxygen Evolution Reaction. *J. Alloys Compd.* **2018,** *731*, 766-773.

6. Wang, J.; Li, L.; Wang, L.; Liu, Y.; Sun, W.; Li, W.; Li, G., In Situ Growth of MoS_2 Nanosheet Arrays and TS_2 (T = Fe, Co, and Ni) Nanocubes onto Molybdate for Efficient Oxygen Evolution Reaction and Improved Hydrogen Evolution Reaction. *ACS Omega* **2018,** *3* (1), 464-471.

7. Seh, Z. W.; Kibsgaard, J.; Dickens, C. F.; Chorkendorff, I.; Norskov, J. K.; Jaramillo, T. F., Combining Theory and Experiment in Electrocatalysis: Insights into Materials Design. *Science* **2017,** *355* (6321), 4998.

8. Favaro, M.; Drisdell, W. S.; Marcus, M. A.; Gregoire, J. M.; Crumlin, E. J.; Haber, J. A.; Yano, J., An Operando Investigation of $(Ni–Fe–Co–Ce)O_x$ System as Highly Efficient Electrocatalyst for Oxygen Evolution Reaction. *ACS Catal.* **2017,** *7* (2), 1248-1258.

9. Ryu, J.; Jung, N.; Jang, J. H.; Kim, H.-J.; Yoo, S. J., In Situ Transformation of Hydrogen-Evolving CoP Nanoparticles: Toward Efficient Oxygen Evolution Catalysts Bearing Dispersed Morphologies with Co-oxo/hydroxo Molecular Units. *ACS Catal.* **2015,** *5* (7), 4066-4074.

10. Fan, H.; Yu, H.; Zhang, Y.; Zheng, Y.; Luo, Y.; Dai, Z.; Li, B.; Zong, Y.; Yan, Q., Fe-Doped Ni_3C Nanodots in N-Doped Carbon Nanosheets for Efficient Hydrogen-Evolution and Oxygen-Evolution Electrocatalysis. *Angew. Chem., Int. Ed. Engl.* **2017,** *129* (41), 12740-12744.

11. Zhao, X.; Zhang, H.; Yan, Y.; Cao, J.; Li, X.; Zhou, S.; Peng, Z.; Zeng, J., Engineering the Electrical Conductivity of Lamellar Silver-Doped Cobalt(II) Selenide Nanobelts for Enhanced Oxygen Evolution. *Angew. Chem., Int. Ed. Engl.* **2017,** *56* (1), 328-332.

12. Li, J.; Liu, G.; Liu, B.; Min, Z.; Qian, D.; Jiang, J.; Li, J., Fe-Doped $CoSe_2$ Nanoparticles Encapsulated in N-Doped Bamboo-Like Carbon Nanotubes as an Efficient Electrocatalyst for Oxygen Evolution Reaction. *Electrochim. Acta* **2018,** *265*, 577-585.

13. Reier, T.; Oezaslan, M.; Strasser, P., Electrocatalytic Oxygen Evolution Reaction (OER) on Ru, Ir, and Pt Catalysts: A Comparative Study of Nanoparticles and Bulk Materials. *ACS Catal.* **2012,** *2* (8), 1765-1772.

14. Antolini, E., Iridium as Catalyst and Cocatalyst for Oxygen Evolution/Reduction in Acidic Polymer Electrolyte Membrane Electrolyzers and Fuel Cells. *ACS Catal.* **2014,** *4* (5), 1426-1440.

15. Anantharaj, S.; Ede, S. R.; Sakthikumar, K.; Karthick, K.; Mishra, S.; Kundu, S., Recent Trends and Perspectives in Electrochemical Water Splitting with an Emphasis on Sulfide, Selenide, and Phosphide Catalysts of Fe, Co, and Ni: A Review. *ACS Catal.* **2016,** *6* (12), 8069-8097.

16. Xu, K.; Cheng, H.; Liu, L.; Lv, H.; Wu, X.; Wu, C.; Xie, Y., Promoting Active Species Generation by Electrochemical Activation in Alkaline Media for Efficient Electrocatalytic Oxygen Evolution in Neutral Media. *Nano Lett.* **2017,** *17* (1), 578-583.

17. Wang, J.; Cui, W.; Liu, Q.; Xing, Z.; Asiri, A. M.; Sun, X., Recent Progress in Cobalt-Based Heterogeneous Catalysts for Electrochemical Water Splitting. *Adv. Mater.* **2016,** *28* (2), 215-30.

18. Zaffran, J.; Stevens, M. B.; Trang, C. D. M.; Nagli, M.; Shehadeh, M.; Boettcher, S. W.; Caspary Toroker, M., Influence of Electrolyte Cations on Ni(Fe)OOH Catalyzed Oxygen Evolution Reaction. *Chem. Mater.* **2017,** *29* (11), 4761-4767.

19. Ganesan, P.; Prabu, M.; Sanetuntikul, J.; Shanmugam, S., Cobalt Sulfide Nanoparticles Grown on Nitrogen and Sulfur Codoped Graphene Oxide: An Efficient Electrocatalyst for Oxygen Reduction and Evolution Reactions. *ACS Catal.* **2015,** *5* (6), 3625-3637.

20. Bates, M. K.; Jia, Q.; Doan, H.; Liang, W.; Mukerjee, S., Charge-Transfer Effects in Ni–Fe and Ni–Fe–Co Mixed-Metal Oxides for the Alkaline Oxygen Evolution Reaction. *ACS Catal.* **2015,** *6* (1), 155-161.

21. Doyle, R. L.; Godwin, I. J.; Brandon, M. P.; Lyons, M. E., Redox and Electrochemical Water Splitting Catalytic Properties of Hydrated Metal Oxide Modified Electrodes. *Phys. Chem. Chem. Phys.* **2013,** *15* (33), 13737-83.

22. Chang, J.; Xiao, Y.; Xiao, M.; Ge, J.; Liu, C.; Xing, W., Surface Oxidized Cobalt-Phosphide Nanorods as an Advanced Oxygen Evolution Catalyst in Alkaline Solution. *ACS Catal.* **2015,** *5* (11), 6874-6878.

23. Liu, D.; Lu, Q.; Luo, Y.; Sun, X.; Asiri, A. M., $NiCo_2S_4$ Nanowires Array as an Efficient Bifunctional Electrocatalyst for Full Water Splitting with Superior Activity. *Nanoscale* **2015,** *7* (37), 15122-15126.

24. Gao, Q.; Wang, X.; Shi, Z.; Ye, Z.; Wang, W.; Zhang, N.; Hong, Z.; Zhi, M., Synthesis of Porous $NiCo_2S_4$ Aerogel for Supercapacitor Electrode and Oxygen Evolution Reaction Electrocatalyst. *Chem. Eng. J.* **2018,** *331*, 185-193.

25. Hou, Y.; Lohe, M. R.; Zhang, J.; Liu, S.; Zhuang, X.; Feng, X., Vertically Oriented Cobalt Selenide/Nife Layered-Double-Hydroxide Nanosheets Supported on Exfoliated Graphene Foil: An Efficient 3d Electrode for Overall Water Splitting. *Energy Environ. Sci.* **2016,** *9* (2), 478-483.

26. Chen, W.; Liu, Y.; Li, Y.; Sun, J.; Qiu, Y.; Liu, C.; Zhou, G.; Cui, Y., In Situ Electrochemically Derived Nanoporous Oxides from Transition Metal Dichalcogenides for Active Oxygen Evolution Catalysts. *Nano Lett.* **2016,** *16* (12), 7588-7596.

27. Jin, Y.; Huang, S.; Yue, X.; Du, H.; Shen, P. K., Mo- and Fe-Modified $Ni(OH)_2$/NiOOH Nanosheets as Highly Active and Stable Electrocatalysts for Oxygen Evolution Reaction. *ACS Catal.* **2018,** *8* (3), 2359-2363.

28. Fang, W.; Liu, D.; Lu, Q.; Sun, X.; Asiri, A. M., Nickel Promoted Cobalt Disulfide Nanowire Array Supported on Carbon Cloth: An Efficient and Stable Bifunctional Electrocatalyst for Full Water Splitting. *Electrochem. Commun.* **2016,** *63*, 60-64.

29. Xu, Y.-Z.; Yuan, C.-Z.; Chen, X.-P., Co-Doped NiSe Nanowires on Nickel Foam Via a Cation Exchange Approach as Efficient Electrocatalyst for Enhanced Oxygen Evolution Reaction. *RSC Adv.* **2016,** *6* (108), 106832-106836.

30. Liu, Q.; Jin, J.; Zhang, J., $NiCo_2S_4$@Graphene as a Bifunctional Electrocatalyst for Oxygen Reduction and Evolution Reactions. *ACS Appl. Mater. Interfaces* **2013,** *5* (11), 5002-5008.

31. Zhao, X.; Yang, Y.; Li, Y.; Cui, X.; Zhang, Y.; Xiao, P., NiCo-Selenide as a Novel Catalyst for Water Oxidation. *J. Mater. Sci.* **2016,** *51* (8), 3724-3734.

32. Liu, T.; Sun, X.; Asiri, A. M.; He, Y., One-Step Electrodeposition of Ni–Co–S Nanosheets Film as a Bifunctional Electrocatalyst for Efficient Water Splitting. *Int. J. Hydrogen Energy* **2016,** *41* (18), 7264-7269.

33. Liu, T.; Asiri, A. M.; Sun, X., Electrodeposited Co-Doped $NiSe_2$ Nanoparticles Film: A Good Electrocatalyst for Efficient Water Splitting. *Nanoscale* **2016,** *8* (7), 3911-3915.

34. Fang, L.; Li, W.; Guan, Y.; Feng, Y.; Zhang, H.; Wang, S.; Wang, Y., Tuning Unique Peapod-Like $Co(S_xSe_{1-x})_2$ Nanoparticles for Efficient Overall Water Splitting. *Adv. Funct. Mater.* **2017,** *27* (24), 1701008.

35. Xia, C.; Jiang, Q.; Zhao, C.; Hedhili, M. N.; Alshareef, H. N., Selenide-Based Electrocatalysts and Scaffolds for Water Oxidation Applications. *Adv. Mater.* **2016,** *28* (1), 77-85.

36. Shinde, D. V.; Trizio, L. D.; Dang, Z.; Prato, M.; Gaspari, R.; Manna, L., Hollow and Porous Nickel Cobalt Perselenide Nanostructured Microparticles for Enhanced Electrocatalytic Oxygen Evolution. *Chem. Mater.* **2017,** *29* (16), 7032-7041.

37. Nikdov, I.; Darkaoui, R.; Zhecheva, E.; Stoyanova, R.; Dimitrov, N.; Vitanov, T., Electrocatalytic Activity of Spine1 Related Cobaltites $M_xCo_{3-x}O_4$ (M = Li, Ni, Cu) in the Oxygen Evolution Reaction. *Electroanal. Chem.* **1997,** *429*, 157-168.

38. Yang, Y.; Fei, H.; Ruan, G.; Xiang, C.; Tour, J. M., Efficient Electrocatalytic Oxygen Evolution on Amorphous Nickel-Cobalt Binary Oxide Nanoporous Layers. *ACS Nano* **2014,** *8* (9), 9518-9523.

39. Chi, J.-Q.; Yan, K.-L.; Xiao, Z.; Dong, B.; Shang, X.; Gao, W.-K.; Li, X.; Chai, Y.-M.; Liu, C.-G., Trimetallic Ni-Fe-Co Selenides Nanoparticles Supported on Carbon Fiber Cloth as Efficient Electrocatalyst for Oxygen Evolution Reaction. *Int. J. Hydrogen Energy* **2017,** *42* (32), 20599-20607.

40. Zhang, J.; Zhang, D.; Zhang, R.; Zhang, N.; Cui, C.; Zhang, J.; Jiang, B.; Yuan, B.; Wang, T.; Xie, H.; Li, Q., Facile Synthesis of Mesoporous and Thin-Walled Ni–Co Sulfide Nanotubes as Efficient Electrocatalysts for Oxygen Evolution Reaction. *ACS Appl. Energy Mater.* **2018,** *1* (2), 495-502.

41. Hu, C.; Zhang, L.; Zhao, Z. J.; Li, A.; Chang, X.; Gong, J., Synergism of Geometric Construction and Electronic Regulation: 3d Se-$(NiCo)S_x/(OH)_x$ Nanosheets for Highly Efficient Overall Water Splitting. *Adv. Mater.* **2018,** *30* (12), 1705538.

42. Tang, C.; Cheng, N.; Pu, Z.; Xing, W.; Sun, X., NiSe Nanowire Film Supported on Nickel Foam: An Efficient and Stable 3d Bifunctional Electrode for Full Water Splitting. *Angew. Chem., Int. Ed.* **2015,** *54* (32), 9351-9355.

43. De Silva, U.; Masud, J.; Zhang, N.; Hong, Y.; Liyanage, W. P. R.; Asle Zaeem, M.; Nath, M., Nickel Telluride as a Bifunctional Electrocatalyst for Efficient Water Splitting in Alkaline Medium. *J. Mater. Chem. A* **2018,** *6* (17), 7608-7622.

44. Umapathi, S.; Masud, J.; Swesi, A. T.; Nath, M., $FeNi_2Se_4$–Reduced Graphene Oxide Nanocomposite: Enhancing Bifunctional Electrocatalytic Activity for Oxygen Evolution and Reduction through Synergistic Effects. *Adv. Sustainable Syst.* **2017,** *1* (10), 1700086.

45. Swesi, A. T.; Masud, J.; Liyanage, W. P. R.; Umapathi, S.; Bohannan, E.; Medvedeva, J.; Nath, M., Textured $NiSe_2$ Film: Bifunctional Electrocatalyst for Full Water Splitting at Remarkably Low Overpotential with High Energy Efficiency. *Sci. Rep.* **2017,** *7* (1), 2401.

46. Zhou, W.; Wu, X.-J.; Cao, X.; Huang, X.; Tan, C.; Tian, J.; Liu, H.; Wang, J.; Zhang, H., Ni_3S_2 Nanorods/Ni Foam Composite Electrode with Low Overpotential for Electrocatalytic Oxygen Evolution. *Energy Environ. Sci.* **2013,** *6* (10), 2921.

47. Ma, Z.; Zhao, Q.; Li, J.; Tang, B.; Zhang, Z.; Wang, X., Three-Dimensional Well-Mixed / Highly-Densed NiS-CoS Nanorod Arrays: An Efficient and Stable Bifunctional Electrocatalyst for Hydrogen and Oxygen Evolution Reactions. *Electrochim. Acta* **2018,** *260*, 82-91.

48. Han, X.; Tong, X.; Wu, G.; Yang, N.; Guo, X.-Y., Carbon Fibers Supported NiSe Nanowire Arrays as Efficient and Flexible Electrocatalysts for the Oxygen Evolution Reaction. *Carbon* **2018,** *129*, 245-251.

49. Liu, T.; Liang, Y.; Liu, Q.; Sun, X.; He, Y.; Asiri, A. M., Electrodeposition of Cobalt-Sulfide Nanosheets Film as an Efficient Electrocatalyst for Oxygen Evolution Reaction. *Electrochem. Commun.* **2015,** *60*, 92-96.

50. Yang, J.; Fujigaya, T.; Nakashima, N., Decorating Unoxidized-Carbon Nanotubes with Homogeneous Ni-Co Spinel Nanocrystals Show Superior Performance for Oxygen Evolution/Reduction Reactions. *Sci. Rep.* **2017,** *7*, 45384.

51. Deng, X.; Ozturk, S.; Weidenthaler, C.; Tuysuz, H., Iron-Induced Activation of Ordered Mesoporous Nickel Cobalt Oxide Electrocatalyst for the Oxygen Evolution Reaction. *ACS Appl. Mater. Interfaces* **2017,** *9* (25), 21225-21233.

52. Chen, W.; Wang, H.; Li, Y.; Liu, Y.; Sun, J.; Lee, S.; Lee, J.-S.; Cui, Y., In Situ Electrochemical Oxidation Tuning of Transition Metal Disulfides to Oxides for Enhanced Water Oxidation. *ACS Cent. Sci.* **2015,** *1* (5), 244-251.

53. Mabayoje, O.; Shoola, A.; Wygant, B. R.; Mullins, C. B., The Role of Anions in Metal Chalcogenide Oxygen Evolution Catalysis: Electrodeposited Thin Films of Nickel Sulfide as "Pre-Catalysts". *ACS Energy Lett.* **2016,** *1* (1), 195-201.

54. Burke, M. S.; Kast, M. G.; Trotochaud, L.; Smith, A. M.; Boettcher, S. W., Cobalt–Iron (Oxy)hydroxide Oxygen Evolution Electrocatalysts: The Role of Structure and Composition on Activity, Stability, and Mechanism. *J. Am. Chem. Soc.* **2015,** *137* (10), 3638-3648.

55. Louie, M. W.; Bell, A. T., An Investigation of Thin-Film Ni–Fe Oxide Catalysts for the Electrochemical Evolution of Oxygen. *J. Am. Chem. Soc.* **2013,** *135* (33), 12329-12337.

56. Friebel, D.; Louie, M. W.; Bajdich, M.; Sanwald, K. E.; Cai, Y.; Wise, A. M.; Cheng, M.-J.; Sokaras, D.; Weng, T.-C.; Alonso-Mori, R.; Davis, R. C.; Bargar, J. R.; Nørskov, J. K.; Nilsson, A.; Bell, A. T., Identification of Highly Active Fe Sites in (Ni,Fe)OOH for Electrocatalytic Water Splitting. *J. Am. Chem. Soc.* **2015,** *137* (3), 1305-1313.

57. Bates, M. K.; Jia, Q.; Doan, H.; Liang, W.; Mukerjee, S., Charge-Transfer Effects in Ni–Fe and Ni–Fe–Co Mixed-Metal Oxides for the Alkaline Oxygen Evolution Reaction. *ACS Catal.* **2016,** *6* (1), 155-161.

58. Smith, R. D. L.; Berlinguette, C. P., Accounting for the Dynamic Oxidative Behavior of Nickel Anodes. *J. Am. Chem. Soc.* **2016,** *138* (5), 1561-1567.

59. Xu, S.-M.; Yan, H.; Wei, M., Band Structure Engineering of Transition-Metal-Based Layered Double Hydroxides toward Photocatalytic Oxygen Evolution from Water: A Theoretical–Experimental Combination Study. *J. Phys. Chem. C* **2017,** *121* (5), 2683-2695.

60. Monteverde Videla, A. H. A.; Stelmachowski, P.; Ercolino, G.; Specchia, S., Benchmark Comparison of Co_3O_4 Spinel-Structured Oxides with Different Morphologies for Oxygen Evolution Reaction under Alkaline Conditions. *J. Appl. Electrochem.* **2017,** *47* (3), 295-304.

61. Friebel, D.; Louie, M. W.; Bajdich, M.; Sanwald, K. E.; Cai, Y.; Wise, A. M.; Cheng, M. J.; Sokaras, D.; Weng, T. C.; Alonso-Mori, R.; Davis, R. C.; Bargar, J. R.; Norskov, J. K.; Nilsson, A.; Bell, A. T., Identification of Highly Active Fe Sites in (Ni,Fe)OOH for Electrocatalytic Water Splitting. *J. Am. Chem. Soc.* **2015,** *137* (3), 1305-1313.

62. Yan, D.; Li, Y.; Huo, J.; Chen, R.; Dai, L.; Wang, S., Defect Chemistry of Nonprecious-Metal Electrocatalysts for Oxygen Reactions. *Adv. Mater.* **2017,** *29* (48), 1606459.

Table of Contents Figure